CARBON 51 (2013) 36–44

Available at www.sciencedirect.com

SciVerse ScienceDirect

journal homepage: www.elsevier.com/locate/carbon

Electrochemically reduced graphene oxide sheets for use in high performance supercapacitors

Jiang Yang, Sundaram Gunasekaran *

Department of Biological Systems Engineering, University of Wisconsin-Madison, 460 Henry Mall, Madison, WI 53706, USA

ARTICLE INFO

Article history:
Received 17 April 2012
Accepted 1 August 2012
Available online 9 August 2012

ABSTRACT

Graphene oxide (GO) was reduced by a rapid, effective and eco-friendly electrochemical method of repetitive cathodic cyclic potential cycling, without using any reducing reagents. The electrochemically reduced graphene oxide (ERGO) was characterized by UV–vis, EIS and zeta-potential measurements. Most of the oxygen functional groups in ERGO were successfully removed resulting in smaller charge transfer resistance. However, some electrochemically stable residuals still remained, enabling ERGO to facilitate electrolyte penetration and pseudocapacitance. Since ERGO was readily stabilized by cathodic potential cycling, it exhibited an outstanding stability in cycle life, nearly with no capacitive loss from the second cycle on. A specific capacitance of 223.6 F g^{-1} was achieved at 5 mV s^{-1}, which makes the ERGO a competitive material for electrochemical energy storage.

1. Introduction

Supercapacitors, also known as electric double-layer capacitors (EDLCs) or ultracapacitors, have attracted much attention from the research community in recent years [1]. These devices can serve as power sources by themselves or in combination with other devices and have many appealing properties such as rapid charging/discharging rate, excellent energy density, high power density and long lifetime, possibly over one million cycles [2]. The energy density of supercapacitors are several orders of magnitude higher than that of conventional dielectric capacitors [3], because energy density is inversely related to the double layer thickness. There are two mechanisms of energy storage in supercapacitors: (1) EDLCs where capacitance is aroused by reversible electrolyte ion adsorption at electrode-electrolyte interface and formation of a double layer with high-surface-area carbon materials as typical examples and (2) redox capacitors where battery-type redox reactions generate pseudocapacitance with certain metal oxides or conducting polymers as electrode materials. There are numerous studies on the development of supercapacitive materials of carbon [3–5], metal oxides [6,7], conducting polymers [8] and composites [9]. Though energy densities based on pseudocapacitance are much higher than that of EDLC, the faradic reactions within pseudocapacitive electrodes can cause phase changes, limiting their lifetime and power densities [10]. Meanwhile, practical applications of pseudocapacitive materials are also confined to their low electrical conductivity, poor compatibility with organic electrolytes [1] and relatively high cost. Therefore, it is essential to look for new, inexpensive, and environmentally friendly energy storage systems.

Carbon materials are known to be the most ideal as supercapacitors to provide DL capacitance [11], with their capacitance directly proportional to surface area and porosity. Different carbon-based materials for high power and energy supercapacitor applications have been extensively reviewed [12,13], including activated carbon, carbon nanotubes, carbon aerogels, graphene and carbon-based composites. Although carbon nanotubes exhibit large surface area, high electrical conductivity along the tubes and good capacitive performance [14], the high cost hinders their commercialization [1]. Graph-

* *Corresponding author.*
E-mail address: guna@wisc.edu (S. Gunasekaran).
0008-6223/$ - see front matter
http://dx.doi.org/10.1016/j.carbon.2012.08.003

ene is a single-atom-thick planar sheet of sp^2-bonded carbon nanostructure with a large theoretical specific surface area of 2630 $m^2 g^{-1}$, high intrinsic in-plane electrical conductivity, and robust mechanical strength [1,10,15]. Graphene materials obtained from GO now can be readily produced and sold by tons at low cost [16]. More importantly, instead of relying on pore distribution in activated carbon (AC), the electronic and capacitance properties of graphene are layer-dependent [17]. Many approaches have been developed to produce graphene physically and chemically such as micromechanical [18] or electrochemical [19] exfoliation, thermally growing from silicon carbide [20], and chemical vapor deposition [21]. Of these, solution-based approach is regarded as the most promising for mass production. Exfoliated GO can be reduced chemically [5,11,22], thermally [23], electrochemically [15,24–26]or by microwave-assisted techniques [1,27]. Considering most reducing reagents such as hydrazine, alkaline, ethylenediamine, $NaBH_4$ and urea are toxic, corrosive or even explosive, there are serious safety and environmental issues. Additionally, possible stabilizers involved in these processes to improve dispersion of reduced GO may be sometimes undesirable due to their degradation on electronic properties [5]. Therefore a greener electrochemical route with the possibility to mass produce is highly desirable. Recently, supercapacitors based on ERGO in aqueous electrolytes using cathodic constant-potential reduction were reported [25,26]. The cycling durability may not be as good as cyclic voltammetry (CV)-reduced GO if without further reduction or manipulation, as capacitance decrease in first multiple cycles were observed [26]. This also widely exists in GO reduced only with one reducing agent [3,5], due to incomplete removal of electrochemically unstable oxygen species.

Herein we report using ERGO, which is reduced from GO by repetitive cathodic cyclic potential cycling, for supercapacitor application in aqueous 1.0 M H_2SO_4 electrolyte. The high negative potential (complete reduced potential: −1.5 V) allowed overcoming energy barriers for oxygen functionalities [24], resulting in the elimination of electrochemically unstable groups. Remaining oxygen groups played a significant role in extra pseudocapacitive effects. During the reduction process, ERGO was readily stabilized electrochemically with barely any capacitive loss for up to 1000 galvanometric cycles. The cyclic voltammetry and galvanostatic charge–discharge results show that ERGO has high gravimetric and volumetric capacitance with satisfactory rate capability and cycling stability.

2. Experimental

2.1. Synthesis of ERGO

GO was synthesized from graphite powder using a modified Hummer's method, and then reduced by intensive repetitive CV cycling as we previously reported [15]. Briefly, 3.0 g graphite powder, 2.5 g $K_2S_2O_8$ and 2.5 g P_2O_5 were mixed with 12 mL 98% H_2SO_4 solution at 80 °C for 4.5 h to obtain pre-oxidized graphite. The mixture was then diluted with 0.5 L water and kept at 80 °C for 12 h. The resulting solution was filtered, washed and vacuum-dried at room temperature overnight. The products were put into 120 mL 98% H_2SO_4 with ice water bath and stirred, followed by gradual addition of 15 g $KMnO_4$ with continuous stirring at 40 °C for 0.5 h and 90 °C for 1.5 h. Further, 250 mL water was added with stirring at 105 °C for 25 min and additionally at room temperature for 2 h. Finally, 0.7 L water and 20 mL 30% (w/w) H_2O_2 were added to terminate the reaction. The as-obtained products were filtered, washed with 3 M HCl solution to remove metal ions, and repeatedly washed with water until neutral pH. It was further purified by dialysis for one week to remove impurities and resuspended by ultrasonication in water to obtain a homogeneous GO solution. Stable exfoliated GO dispersion was achieved by the negative electrostatic repulsion from ionization of carboxyl and phenolic hydroxyl groups of GO and therefore made it much easier to be used for electrode coating and modification compared to comparatively insoluble reduced GO. Glassy carbon electrode (GCE, 3 mm in diameter) was used as the conductive substrate. It was carefully polished on a fine microcloth successively with 0.3 and 0.05 μm alumina slurry (Beuhler) until a mirror-shine surface was obtained, and then rinsed with water. A sonication step was performed consecutively in ethanol and water, and the GCE was then dried at room temperature. Three milliliters GO solution of 1 mg mL^{-1} concentration was drop coated on a conductive electrode surface (e.g. GCE, Au) and dried under ambient conditions. GO was electrochemically reduced by CV scanning from 0.0 to −1.5 V in N_2-purged 0.05 M pH 5.0 PBS (Na_2HPO_4/NaH_2PO_4) for 100 cycles, and then rinsed with water and dried at room temperature. Large-scale electrochemical reduction of GO was performed using the same repetitive cyclic potential sweeping in 3-electrode configuration under the same conditions for longer period of time sealed to minimize evaporations. Doubly-distilled Milli-Q water (18.2 MΩ) was used throughout the study.

2.2. Instrumentation

Hitachi S-4800 (Hitachi, Japan) scanning electron microscope (SEM) was employed for characterizing surface morphology and UV–vis spectra were recorded with Cary 50 Bio UV–vis spectrophotometer (Varian, CA, USA). Zeta potentials were measured using 90Plus particle size analyzer with BI-Zeta option (Brookhaven Instruments Corporation, TX, USA). All electrochemical tests including CV, galvanostatic charge/discharge and EIS were carried out using CHI 660D electrochemical analyzer (CH Instruments, TX, USA) at ambient temperature (25 ± 1 °C) in a three-electrode configuration, with Pt wire counter electrode (CE), saturated Ag/AgCl (3 M KCl) reference electrode (RE) and ERGO as the working electrode (WE). 1 M H_2SO_4 was used as electrolytes and electrochemical impedance spectroscopy (EIS) was conducted from 0.1 Hz to 100 kHz with 5 mV AC perturbation in 1.0 M KCl containing equimolar $K_4[Fe(CN)_6]/K_3[Fe(CN)_6]$ redox probes at open circuit potential.

3. Results and discussion

3.1. Characterizations of ERGO

The surface morphology of ERGO characterized by SEM is shown in Fig. 1A. A few layers of GO sheets appear partially packed with their basal planes, intensely crumpled and

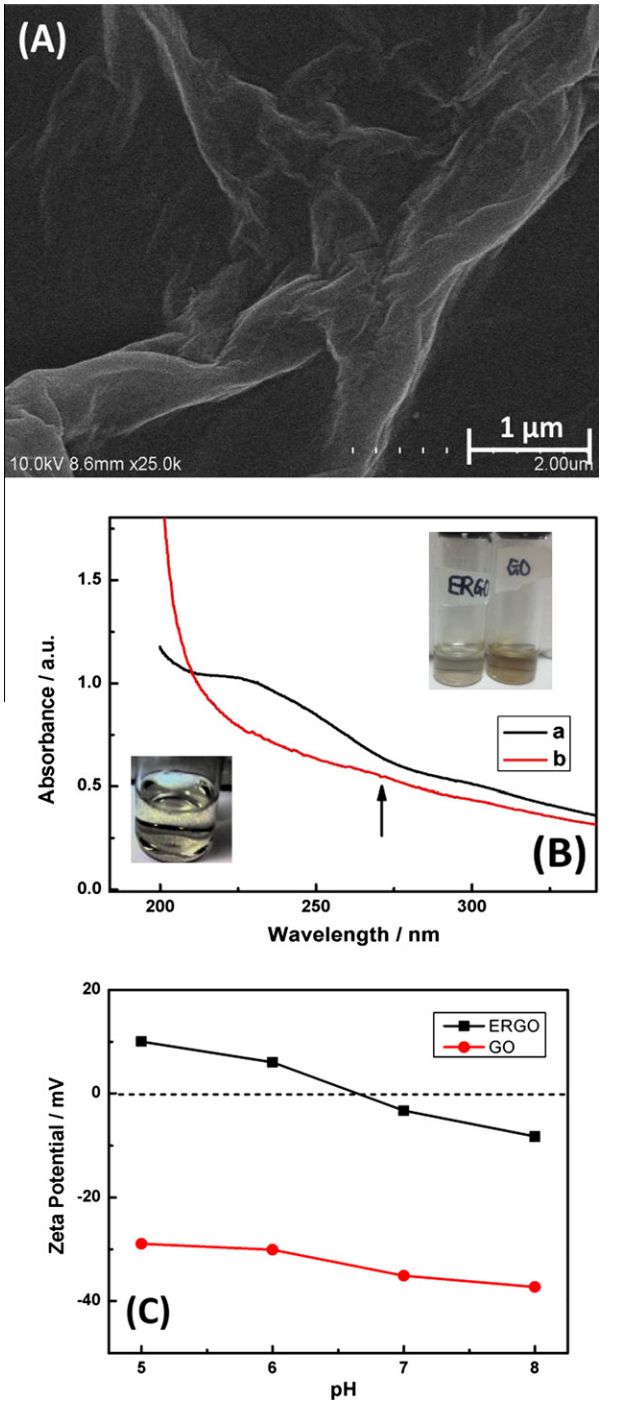

Fig. 1 – (A) SEM image of ERGO. (B) UV–vis spectra of 20 μg mL^{-1} (a) GO and (b) ERGO. Upper right photographs shows the appearance of GO and ERGO solutions while lower left is the magnification of ERGO solution. (C) Zeta potentials of (●) GO and (■) ERGO under different pH.

folded into a typical wrinkled structure after electrochemical reduction, similar to that of reduced GO sheets derived chemically [22], thermally [23] or with microwave [27]. These geometric wrinkling and rippling are caused by nanoscale interlocking of GO sheets, providing enhanced mechanical properties, reduced surface energy, increased surface roughness and area [28]. Corrugated ERGO sheets are arranged intermittently edge-to-edge with less wrinkled or flat sheets, forming an interconnected film parallel to the substrate. We previously reported that ERGO is composed of multilayers of graphene sheets overlapped in parallel for interpenetration [15]. Its properties possibly allow the design of thin-film supercapacitor devices. The corrugations in graphene sheets can cause electron transfer rates 10-fold faster than at the basal plane of graphite [29].

The change in GO after electrochemical reduction was monitored by UV–vis spectroscopy (Fig. 1B). An obvious absorption peak at 230 nm was observed for GO, corresponding to the $\pi \rightarrow \pi^*$ transition of aromatic C–C bonds [5]. After electrochemical reduction, this absorption peak has red-shifted to 270 nm in decreased intensity (as the arrow indicated), indicating restored π conjugation within ERGO sheets [30]. The spectra are close to those from hydrazine reduction [22]. When dispersed in aqueous solution, GO showed a brown color with good dispersion and stability which can last for months, due to the abundant oxygenated groups on the basal plane and edge of GO surface (Fig. 1B upper right inset). In contrast, ERGO exhibited a slightly black color in the solution and many insoluble small particles are visually observable. The increase in hydrophobicity suggested the successful elimination of electrochemically unstable oxygen-containing functional groups after reduction.

To further explore the surface properties, zeta potentials were measured as a function of pH (Fig. 1C). In the pH ranging from 5 to 8, the zeta potential values of GO sheets decreased from −29.0 to −37.3 mV and GO remained highly negatively charged all through, which can be attributed to the presence of oxygen species on the surface. The increase of negative charge in zeta potential at pH 8 is caused by deprotonation of carboxyl groups into carboxylate groups. From a general colloidal science perspective, zeta potentials with absolute values larger than 30 mV can result in a stable dispersion [31]. Therefore, the GO dispersion can be well maintained due to the electrostatic repulsion as observed in Fig. 1B. On the other hand, ERGO showed zeta potential values around zero. The small positive zeta potential values of ERGO at pH < 7 are ascribed to adsorption of positively charged ions (e.g. H^+, Na^+) in the aqueous solution, as a result of removal of negatively charged oxygenated species, also observed in thermally and chemically reduced GO [32]. These results are indicative of efficient electrochemical reduction of GO.

3.2. *Electrochemical characterizations of ERGO*

As the typical method for evaluating the electron transfer properties in carbon materials, CV analysis of redox reactions of $Fe(CN)_6^{3-}/Fe(CN)_6^{4-}$ was used to investigate the intrinsic electrochemical behaviors of ERGO electrode (Fig. 2A). At the same scan rate of 100 mV s^{-1}, ERGO electrode showed a much smaller peak-to-peak potential separation (ΔE_p) and a larger peak current than GO electrode, thus offering a faster electron transfer rate and larger effective surface area at ERGO. The well-defined redox peak pair demonstrates a favorable direct electron transfer between ERGO electrode and redox species [33]. As the scan rate increased, the anodic peak shifted positively while the cathodic peak shifted negatively, generat-

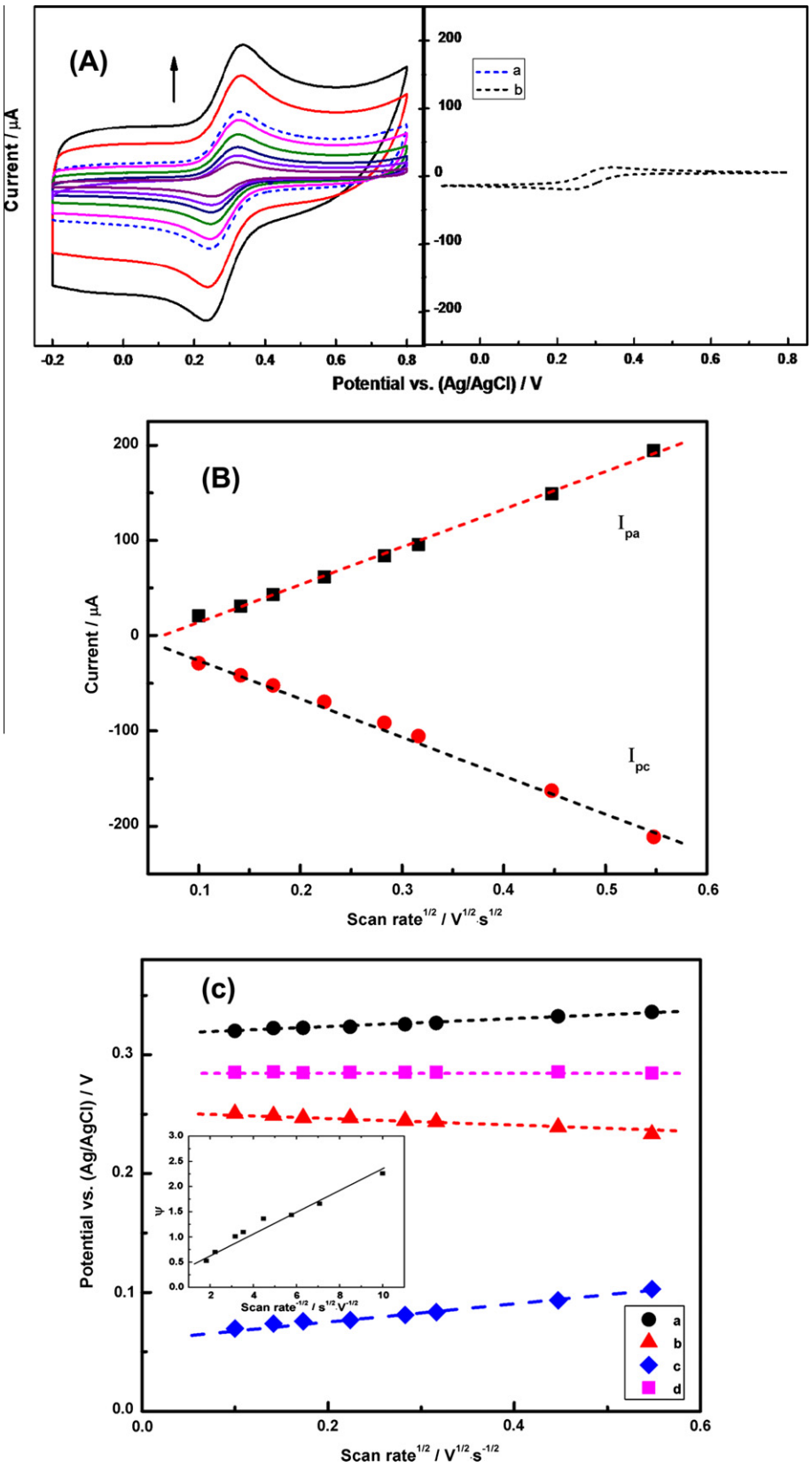

Fig. 2 – (A) Cyclic voltammograms of (a) ERGO (b) GO and in 5.0 mM $K_3[Fe(CN)_6]$ containing 1.0 M KCl at scan rate of 100 mV s^{-1}. Left figure shows ERGO at different scan rates of 10, 20, 30, 50, 80, 100, 200 and 300 mV s^{-1}, with the arrow indicating increasing scan rates. (B) Plot of peak currents vs. square root of scan rates. (C) Plot of anodic and cathodic peak potentials (a and b), potential separation (c), and midpoint potential (d, nearly independent) vs. square root of scan rates. Inset shows ψ vs. reciprocal of square root of scan rate.

ing slightly larger ΔE_p (from 70 to 103 mV) with increasing scan rates which indicated quasi-reversible kinetics at ERGO surface likely as a result of graphite basal plane structures and edge-plane defects [34]. Meanwhile, a linear dependence can be established between the peak currents and square root of scan rates from 0.01 to 0.30 V s^{-1} (R = 0.9985 and 0.9972 and linear Randles' slope of 5.89×10^{-4} and -6.15×10^{-4} for anodic and cathodic peaks, respectively), suggesting a diffusion-controlled non-surface process (Fig. 2B). On the basis of this linear dependency in the one-electron process and Randles-Sevcik equation (Eq. (1)) for quasi-reversible processes [35], the effective surface area (A) of ERGO electrode was calculated as 0.106 ± 0.003 cm^2.

$$Ip = (2.65 \times 10^5) n^{3/2} A D^{1/2} C^* v^{1/2} \quad (1)$$

where, D is diffusion coefficient (cm^2 s^{-1}), C^* is concentration of probe molecule (5×10^{-6} mol cm^{-3}), n is the number of electrons (=1). The result is apparently larger than the geometric area of the electrode (0.071 cm^2) by providing additional electroactive sites and more effective contacts with redox species. Using Nicholson's method [33,36] in which ΔE_p is a function of the dimensionless kinetic parameter ψ, a further linear relation (R = 0.984) can be found for ψ vs. $v^{1/2}$ (Fig. 2C inset), related by k^0 as Eq. (2):

$$\psi = k^0 \left(\frac{D_0}{D_R}\right)^{\alpha/2} \sqrt{RT/(\pi n F D)} v^{-1/2} \quad (2)$$

where, α is the electron transfer coefficient (assumed as 0.5), D_0 is the diffusion coefficient for $K_3[Fe(CN)_6]$ (0.76×10^{-5} cm^2 s^{-1}), D_R is the diffusion coefficient for $K_4[Fe(CN)_6]$, R, T (298 K), π and F have their usual meanings. The standard heterogeneous rate constant k^0 was then estimated as 6.04×10^{-3} cm s^{-1} from the slope of the above linear fit. This value is close to or higher than that of ferricyanide for multilayer graphite [37], monolayer of mechanically exfoliated graphene [38], bare and modified Au electrodes [39], and commercial screen-printed graphite electrodes [35]. Recent studies have suggested that graphene might have more favorable electron transfer kinetics over graphite [40]. Moreover, linear relationships of both E_{pa} and E_{pc}(and ΔE_p) on $v^{1/2}$ (Fig. 2C) were found with close absolute values of slopes, and thus the formal potential or midpoint potential ($\frac{E_{pa}+E_{pc}}{2}$) is independent of scan rates suggesting characteristics of the redox reaction and good association of ERGO with electrode surface in the solution conditions. Considering ψ vs. $v^{1/2}$ was also linear, a linear relationship of ΔE_p on ψ^{-1} can be built consistent with the model of alternative Nicholson's working curve developed by Paul et al. for quasi-reversible process [41].

The electron transfer characteristics between electrolyte and electrode interfacial surface were studied using EIS in 0.01 M $[Fe(CN)_6]^{3-/4-}$ as shown by the Nyquist complex-plane plots (Fig. 3). The semicircular part in the high frequency region (Fig. 3 inset) represents electron-transfer-limiting process with its effective diameter equal to the faradic charge transfer resistance (R_{ct}) which is responsible to the electron transfer kinetics of redox reactions at the electrode-electrolyte interface. It is obvious that GO exhibited a much larger R_{ct} than bare electrode, due to the presence of excessive oxygenated species which arouse insulating characteristics and hinder its electrochemical properties [11]. ERGO, on the other hand,

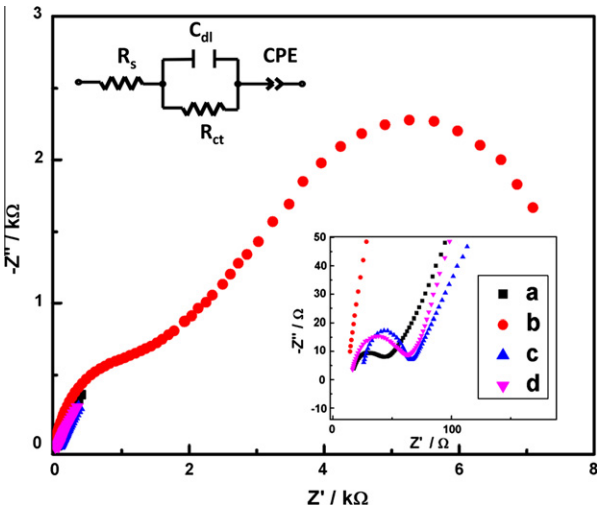

Fig. 3 – Nyquist plots of (a) ERGO, (b) GO, (c) bare, (d) ERGO after 1000 charge/discharge cycles in 1.0 M KCl containing 0.01 M $K_4[Fe(CN)_6]/K_3[Fe(CN)_6]$. Lower right inset: enlarged high-frequency region. Upper left inset: equivalent circuit $[R_s(C_{dl}R_{ct})]$CPE fitting ERGO electrode. R_s: solution resistance, R_{ct}: electron transfer resistance, C_{dl}: double layer capacitance, CPE: constant phase element.

displayed a significantly reduced R_{ct} (29.7 Ω) than GO, suggesting enhanced electronic properties and successful elimination of electrochemically unstable oxygen species during reduction, which can cause pseudocapacitance [11]. From the intercept at real part equal to internal resistance (R_i), ERGO has the smallest value indicating ERGO can achieve higher charge/discharge rate and the removed oxygen species in GO mainly contribute to the increase of R_{ct} rather than R_i. Furthermore, the straight line in the low frequency region, corresponding to a diffusion-limiting process, is less inclined for ERGO, suggesting more closely ideal capacitor behaviors [10] possibly by forming more uniform diffusion paths for protons within ERGO after reduction. GO electrode, however, displayed a particularity with a second semicircle in the low frequency region which is the typical characteristic of diffusion through a finite length diffusion layer. Hereby, the non-ideal line of ERGO can be expressed by the serial constant phase element (CPE) as in the equivalent circuit with the parameter CPE-P = 0.50 identical to a Warburg element, demonstrating ideal C_{dl} only accounts for part of the capacitive performance. After 1000 charge/discharge cycles, R_{ct} of ERGO increased to 52.5 Ω owing to fewer hopping sites of oxygenated groups on ERGO in slow kinetics faradic reactions after long cycling period [42], similar to chemically reduced RGO behaviors [11]. The solution resistance (R_s) only varied a little (2.9%) after 1000 cycles due to its relative insensitivity to electrode surface.

3.3. *Capacitive properties of ERGO*

The capacitive behavior of ERGO was evaluated with 3-electrode configuration in aqueous system at 100 mV s^{-1} (Fig. 4A). Both GO and GC electrodes presented negligible current responses, whereas a remarkably large current was seen in

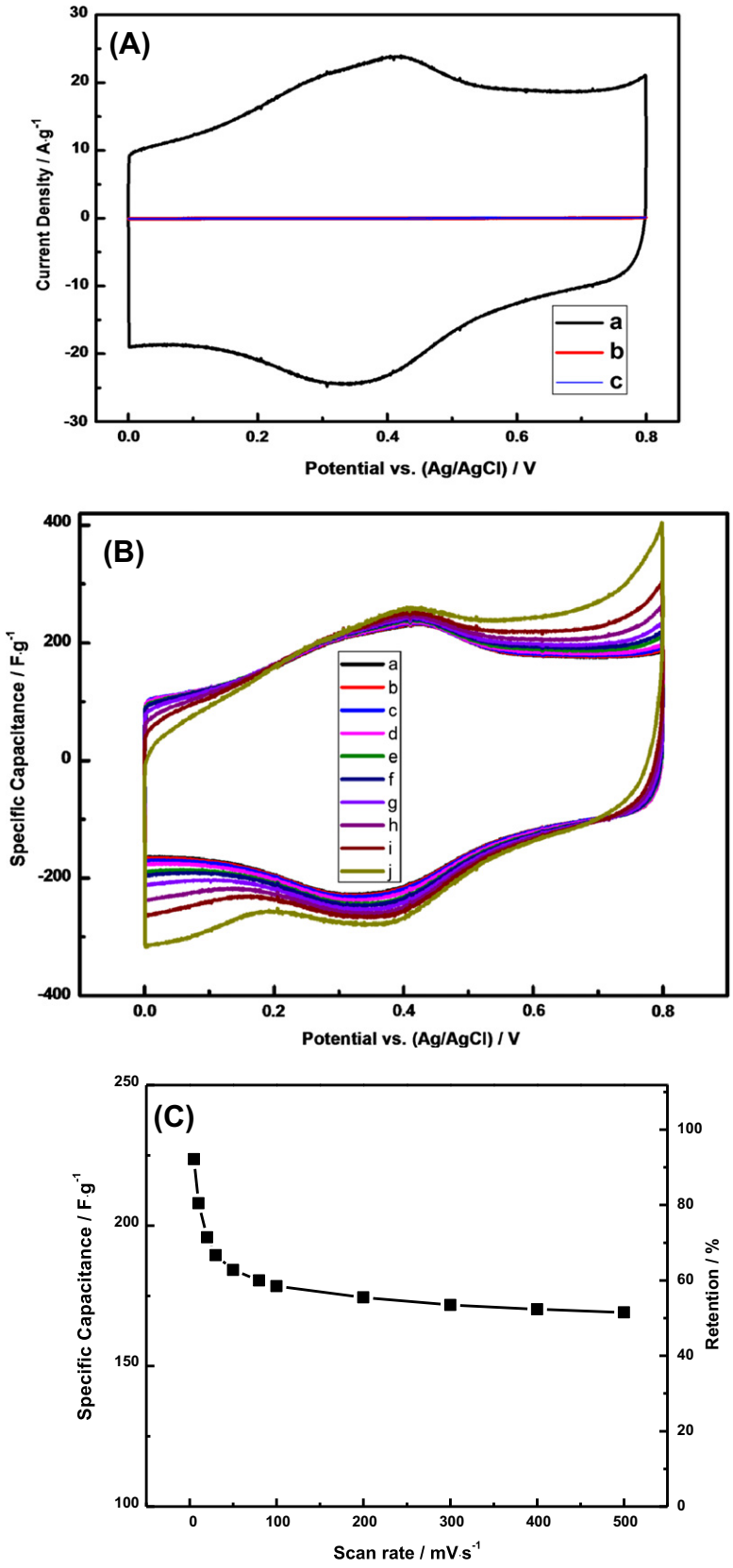

Fig. 4 – (A) Cyclic voltammograms of (a) ERGO (b) GC and (c) GO electrodes. Scan rate: 100 mV s^{-1}. (B) Cyclic voltammograms of ERGO at different scan rate from 10 to 500 mV s^{-1} (from j to a). (C) Capacitance retention ratio and specific capacitance as a function of scan rate from 5 to 500 mV s^{-1}. Electrolyte: 1.0 M H_2SO_4.

the CV profile of ERGO, which showed a typical rectangular shape indicating an excellent capacitive behavior. At the same time, a pair of redox peaks were found, attributed to quinone/hydroquinone groups typically in carbon materials [43]. This confirmed the residual electrochemically stable oxygen groups are still actively involved in faradic redox reactions and contribute to pseudocapacitance of ERGO, though the reduction of electrochemically unstable oxygen groups greatly increased capacitance. Additionally, the unremoved oxygen groups can also increase hydrophilicity of ERGO to some degree (we have reported a water contact angle of 72° [15]), allowing penetration of aqueous electrolyte [11].

CV curves of ERGO electrodes were obtained at scan rates from 5 to 500 mV s^{-1} (Fig. 4B). The current response increased with scan rates and similar rectangular shape with a pair of redox peaks is observed at all scan rates, with no obvious distortion (even at a scan rate of 10 V s^{-1}, no obvious distortion is observed). This superior acceptable capacitive performance is due to the partial restoration of π-conjugation structure and improved electronic conductivity. The specific capacitance (C_m) of ERGO from CV can be calculated from Eq. (3):

$$C_m = \frac{|Q_f| + |Q_b|}{2m\Delta V} \quad (3)$$

where, Q_f and Q_b are voltammetric charge integrated from area of forward and backward scans under CV curves, respectively; m is the mass of electrode materials; ΔV is the potential window. The capacitance and retention ratio (of C_m at 5 mV s^{-1}) of ERGO as a function of scan rate are shown in Fig. 4C. At 5 mV s^{-1}, a specific capacitance of 223.6 F g^{-1} was obtained and this value decreased with increasing scan rate, first dramatically and then gradually until a relatively stable value (~170 F g^{-1}) was reached, showing great rate capability. The rapid decrease is because some oxygen groups that are still remaining on ERGO are unable to participate in faradic redox reactions at higher scan rates, leading to lower pseudocapacitance [5]. This phenomenon can also be seen in Fig. 4B from decreasing redox peak area with increasing scan rate. At 500 mV s^{-1}, 75.6% of C_m can be maintained, while 178.4 F g^{-1} (80.0%) can be achieved at 100 mV s^{-1}. This capacitance performance is a better than those of GO reduced by hydrobromic acid [11], GO reduced by microwave-solvothermal route with hydrazine [44], hydrogen-induced exfoliated graphene [45], and inkjet-printed and thermally reduced GO in the same electrolyte [4]. Compared with other carbon materials, the specific capacitance is higher than nanodiamond and onion-like-carbon (OLC) in the range of 20–40 F g^{-1} [46], and the low capacitance of OLC is said to be caused by its hydrophobic surface making it difficult to be dispersed in aqueous solution and/or to be accessed by aqueous electrolyte. It is also higher than mesoporous carbon synthesized from silica templates ranging from 114 to 147 F g^{-1} [47] and is comparable to nanoporous carbon activated of ~240 F g^{-1} at temperature above 950 °C [48]. Galvanostatic charge/discharge performance of ERGO electrode was tested at different current densities (Fig. 5A). Symmetric charge/discharge curves of almost linear potential variation in good triangle shape revealed a good capacitive performance from electrical double layer capacitance and pseudocapacitance. The specific capacitance here is calculated depending on Eq. (4):

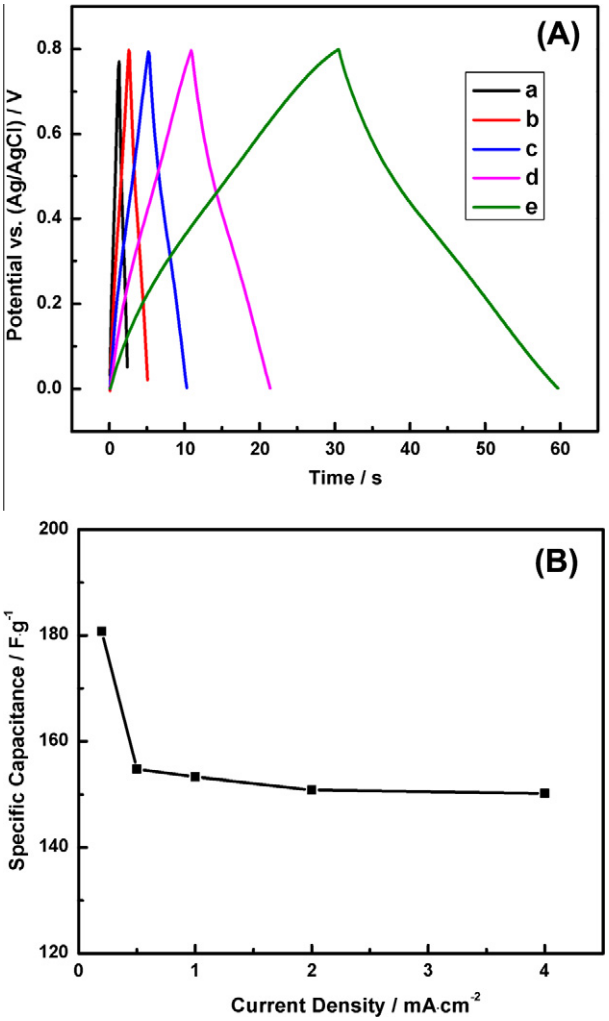

Fig. 5 – (A) Galvanostatic charge/discharge curves of ERGO-based supercapacitor in 1.0 M H_2SO_4 at different current densities of (a) 4, (b) 2, (c) 1, (d) 0.5 and (e) 0.2 mA cm^{-2}. (B) Dependence of capacitance of ERGO supercapacitor on current density. Potential range: 0–0.8 V.

$$C_m = \frac{I\Delta t}{\Delta V m} \quad (4)$$

where, I is the discharged current, Δt is the discharging time and other parameters have identical meanings as before. The highest C_m of 180.8 F g^{-1} at 0.2 mA cm^{-2} is ascribed to the remaining electrochemically stable oxygen species in ERGO generating extra pseudocapacitance and facilitated electrolyte penetration [11]. C_m gradually decreased with increase of discharging current densities, and stabilized around 150 F g^{-1} (Fig. 5B). This decrease, though small (~2.9% loss in capacitance from 0.5 to 4 mA cm^{-2}), is generally caused by internal resistance drop (IR drop). The IR drop was observed to be 3.5 mV at 0.2 mA cm^{-2} resulting in the low capacitance loss.

The cycle life of the supercapacitor as an important factor for practical applications[3] was examined at current density of 0.2 mA cm^{-2} for up to 1000 charge/discharge cycles (Fig. 6A). The specific capacitance of ERGO electrode was 207.8 F g^{-1} in the first cycle and remained almost constant around 180 F g^{-1}

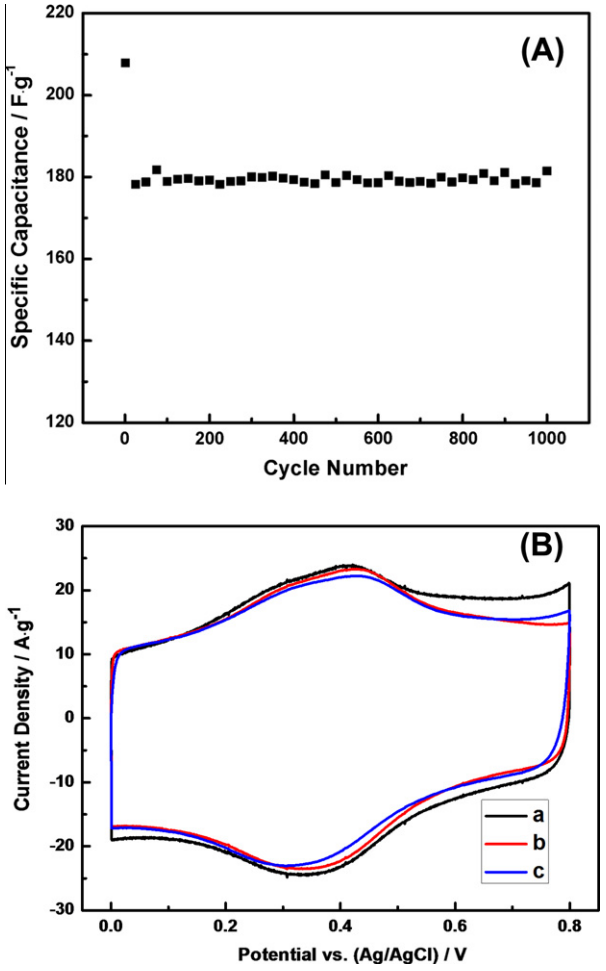

Fig. 6 – (A) Cycle life of ERGO electrode at the current density of 0.2 mA cm^{-2} between 0 and 0.8 V. (B) Cyclic voltammograms in 1.0 M H_2SO_4 at 100 mV s^{-1} of (a) ERGO electrode, (b) after 1000 charge/discharge cycles and (c) after storage for 1 week.

from the second cycle on, revealing extraordinary capacitive stability and high level of reversibility in repetitive charge/discharge cycling. This strong stability is because during the electrochemical reduction, ERGO has already been stabilized with those electrochemically unstable deteriorating oxygen species removed. Given the fact that GO with high oxygen contents does not have a comparable capacitance (Fig. 4A), it can be inferred that the residual covalently bonded oxygen species in ERGO are reversible, stable and desirable, playing an important part in its excellent performance. The CV curves of ERGO electrode after 1000 cycles and one week storage (with a tight plastic cap kept from air) were also compared to estimate the retention ability (Fig. 6B). Virtually very little loss in capacitance can be seen and therefore ERGO is suitable for high-performance supercapacitor applications.

4. Summary

We have demonstrated the supercapacitive application of ERGO obtained by reducing GO by an easy, cost-effective and eco-friendly electrochemical method without using any reducing agents. After reduction, π-conjugated structure in graphene was repaired and electrochemically unstable oxygen groups were rapidly removed, yielding greatly improved electron transfer kinetics and capacitive properties of ERGO. Meanwhile, residual oxygen groups on ERGO are considerably stable and reversible in capacitive performance providing additional faradic pseudocapacitance without damaging its electronic properties. The supercapacitor was readily stabilized during reduction. A specific capacitance of 223.6 F $g^{-1}$was achieved at 5 mV s^{-1}, while a gravimetric value of 180.8 F g^{-1} at 0.2 mA cm^{-2} could be well maintained up to 1000 cycles. The superior and stable capacitive performance renders ERGO as a promising material for energy storage.

Acknowledgements

This research was financially supported by a Federal HATCH grant from College of Agricultural and Life Sciences at the University of Wisconsin-Madison.

REFERENCES

[1] Zhu YW, Murali S, Stoller MD, Ganesh KJ, Cai WW, Ferreira PJ, et al. Carbon-based supercapacitors produced by activation of graphene. Science 2011;332(6037):1537–41.
[2] Miller JR, Outlaw RA, Holloway BC. Graphene double-layer capacitor with ac line-filtering performance. Science 2010;329(5999):1637–9.
[3] Wang Y, Shi Z, Huang Y, Ma Y, Wang C, Chen M, et al. Supercapacitor devices based on graphene materials. J Phys Chem C 2009;113(30):13103–7.
[4] Le LT, Ervin MH, Qiu H, Fuchs BE, Lee WY. Graphene supercapacitor electrodes fabricated by inkjet printing and thermal reduction of graphene oxide. Electrochem Commun 2011;13(4):355–8.
[5] Lei ZB, Lu L, Zhao XS. The electrocapacitive properties of graphene oxide reduced by urea. Energy Environ Sci 2012;5(4):6391–9.
[6] Patake VD, Lokhande CD, Joo OS. Electrodeposited ruthenium oxide thin films for supercapacitor: effect of surface treatments. Appl Surf Sci 2009;255(7):4192–6.
[7] Toupin M, Brousse T, Bélanger D. Charge storage mechanism of MnO_2 electrode used in aqueous electrochemical capacitor. Chem Mater 2004;16(16):3184–90.
[8] Snook GA, Kao P, Best AS. Conducting-polymer-based supercapacitor devices and electrodes. J Power Sources 2011;196(1):1–12.
[9] Lang X, Hirata A, Fujita T, Chen M. Nanoporous metal/oxide hybrid electrodes for electrochemical supercapacitors. Nat Nanotechnol 2011;6(4):232–6.
[10] Stoller MD, Park S, Zhu Y, An J, Ruoff RS. Graphene-based ultracapacitors. Nano Lett 2008;8(10):3498–502.
[11] Chen Y, Zhang X, Zhang D, Yu P, Ma Y. High performance supercapacitors based on reduced graphene oxide in aqueous and ionic liquid electrolytes. Carbon 2011;49(2):573–80.
[12] Simon P, Gogotsi Y. Materials for electrochemical capacitors. Nat Mater 2008;7(11):845–54.
[13] Zhang LL, Zhao XS. Carbon-based materials as supercapacitor electrodes. Chem Soc Rev 2009;38(9):2520–31.

[14] Nie HG, Yao Z, Zhou XM, Yang Z, Huang SM. Nonenzymatic electrochemical detection of glucose using well-distributed nickel nanoparticles on straight multi-walled carbon nanotubes. Biosens Bioelectron 2011;30(1):28–34.
[15] Yang J, Deng SY, Lei JP, Ju HX, Gunasekaran S. Electrochemical synthesis of reduced graphene sheet-AuPd alloy nanoparticle composites for enzymatic biosensing. Biosens Bioelectron 2011;29(1):159–66.
[16] Segal M. Selling graphene by the ton. Nat Nanotechnol 2009;4(10):612–4.
[17] Zhao S, Lv Y, Yang X. Layer-dependent nanoscale electrical properties of graphene studied by conductive scanning probe microscopy. Nanoscale Res Lett 2011;6(1):498.
[18] Novoselov KS, Geim AK, Morozov SV, Jiang D, Zhang Y, Dubonos SV, et al. Electric field effect in atomically thin carbon films. Science 2004;306(5696):666–9.
[19] Su C-Y, Lu A-Y, Xu Y, Chen F-R, Khlobystov AN, Li L-J. High-quality thin graphene films from fast electrochemical exfoliation. ACS Nano 2011;5(3):2332–9.
[20] Berger C, Song Z, Li X, Wu X, Brown N, Naud C, et al. Electronic confinement and coherence in patterned epitaxial graphene. Science 2006;312(5777):1191–6.
[21] Obraztsov AN. Chemical vapour deposition: making graphene on a large scale. Nat Nanotechnol 2009;4(4):212–3.
[22] Choi E-Y, Han TH, Hong J, Kim JE, Lee SH, Kim HW, et al. Noncovalent functionalization of graphene with end-functional polymers. J Mater Chem 2010;20(10):1907–12.
[23] Zhu Y, Stoller MD, Cai W, Velamakanni A, Piner RD, Chen D, et al. Exfoliation of graphite oxide in propylene carbonate and thermal reduction of the resulting graphene oxide platelets. ACS Nano 2010;4(2):1227–33.
[24] Guo H-L, Wang X-F, Qian Q-Y, Wang F-B, Xia X-H. A green approach to the synthesis of graphene nanosheets. ACS Nano 2009;3(9):2653–9.
[25] Sun A, Zheng J, Sheng Q. A highly sensitive non-enzymatic glucose sensor based on nickel and multi-walled carbon nanotubes nanohybrid films fabricated by one-step co-electrodeposition in ionic liquids. Electrochim Acta 2012;65:64–9.
[26] Peng X-Y, Liu X-X, Diamond D, Lau KT. Synthesis of electrochemically-reduced graphene oxide film with controllable size and thickness and its use in supercapacitor. Carbon 2011;49(11):3488–96.
[27] Zhu Y, Murali S, Stoller MD, Velamakanni A, Piner RD, Ruoff RS. Microwave assisted exfoliation and reduction of graphite oxide for ultracapacitors. Carbon 2010;48(7):2118–22.
[28] Chen Z, Ren W, Gao L, Liu B, Pei S, Cheng H-M. Three-dimensional flexible and conductive interconnected graphene networks grown by chemical vapour deposition. Nat Mater 2011;10(6):424–8.
[29] Li W, Tan C, Lowe MA, Abruña HD, Ralph DC. Electrochemistry of individual monolayer graphene sheets. ACS Nano 2011;5(3):2264–70.
[30] Li D, Muller MB, Gilje S, Kaner RB, Wallace GG. Processable aqueous dispersions of graphene nanosheets. Nat Nanotechnol 2008;3(2):101–5.
[31] Choi BG, Park H, Park TJ, Yang MH, Kim JS, Jang S-Y, et al. Solution chemistry of self-assembled graphene nanohybrids for high-performance flexible biosensors. ACS Nano 2010;4(5):2910–8.
[32] Goncalves G, Marques PAAP, Granadeiro CM, Nogueira HIS, Singh MK, Grácio J. Surface modification of graphene nanosheets with gold nanoparticles: the role of oxygen moieties at graphene surface on gold nucleation and growth. Chem Mater 2009;21(20):4796–802.
[33] Bard AJF LR. Electrochemical Methods: Fundamentals and Applications. New York: Wiley; 2000.
[34] Li J, Cassell A, Delzeit L, Han J, Meyyappan M. Novel three-dimensional electrodes: electrochemical properties of carbon nanotube ensembles. J Phys Chem B 2002;106(36):9299–305.
[35] Kadara RO, Jenkinson N, Banks CE. Characterisation of commercially available electrochemical sensing platforms. Sens Actuators B: Chem 2009;138(2):556–62.
[36] Nicholson RS. Theory and application of cyclic voltammetry for measurement of electrode reaction kinetics. Anal Chem 1965;37(11):1351–5.
[37] Mirkin MV, Bard AJ. Simple analysis of quasi-reversible steady-state voltammograms. Anal Chem 1992;64(19):2293–302.
[38] Valota AT, Kinloch IA, Novoselov KS, Casiraghi C, Eckmann A, Hill EW, et al. Electrochemical behavior of monolayer and bilayer graphene. ACS Nano 2011;5(11):8809–15.
[39] He H, Xie Q, Zhang Y, Yao S. A simultaneous electrochemical impedance and quartz crystal microbalance study on antihuman immunoglobulin G adsorption and human immunoglobulin G reaction. J Biochem Biophys Methods 2005;62(3):191–205.
[40] Shao Y, Wang J, Wu H, Liu J, Aksay IA, Lin Y. Graphene based electrochemical sensors and biosensors: a review. Electroanal 2010;22(10):1027–36.
[41] Paul HJ, Leddy J. Direct determination of the transfer coefficient from cyclic voltammetry: isopoints as diagnostics. Anal Chem 1995;67(10):1661–8.
[42] Ghaemi M, Ataherian F, Zolfaghari A, Jafari SM. Charge storage mechanism of sonochemically prepared MnO2 as supercapacitor electrode: effects of physisorbed water and proton conduction. Electrochim Acta 2008;53(14):4607–14.
[43] Wang D-W, Li F, Zhao J, Ren W, Chen Z-G, Tan J, et al. Fabrication of graphene/polyaniline composite paper via in situ anodic electropolymerization for high-performance flexible electrode. ACS Nano 2009;3(7):1745–52.
[44] Murugan AV, Muraliganth T, Manthiram A. Rapid, facile microwave-solvothermal synthesis of graphene nanosheets and their polyaniline nanocomposites for energy strorage. Chem Mater 2009;21(21):5004–6.
[45] Mishra AK, Ramaprabhu S. Functionalized graphene-based nanocomposites for supercapacitor application. J Phys Chem C 2011;115(29):14006–13.
[46] Kovalenko I, Bucknall DG, Yushin G. Detonation nanodiamond and onion-like-carbon-embedded polyaniline for supercapacitors. Adv Funct Mater 2010;20(22):3979–86.
[47] Fuertes AB, Lota G, Centeno TA, Frackowiak E. Templated mesoporous carbons for supercapacitor application. Electrochim Acta 2005;50(14):2799–805.
[48] Janes A, Kurig H, Lust E. Characterisation of activated nanoporous carbon for supercapacitor electrode materials. Carbon 2007;45(6):1226–33.